Label Free Process Monitoring of 3D Bioprinted Engineered Constructs via Dielectric Impedance Spectroscopy

Lokesh Karthik Narayanan^{1,3}, Trevor L. Thompson^{1,3}, Rohan A. Shirwaiker^{1,2,3*}, Binil Starly^{1,2,3*}

¹Edward P. Fitts Department of Industrial and Systems Engineering,

²UNC-NCSU Joint Department of Biomedical Engineering

³Comparative Medicine Institute,

North Carolina State University, Raleigh, NC 27695

Email Correspondence: <u>bstarly@ncsu.edu</u>; <u>rashirwaiker@ncsu.edu</u>

Abstract

Biofabrication processes can affect biological quality attributes of encapsulated cells within constructs. Currently, assessment of the fabricated constructs is performed offline by subjecting the constructs to destructive assays that require staining and sectioning. This drawback limits the translation of biofabrication processes to industrial practice. In this work, we investigate the dielectric response of viable cells encapsulated in bioprinted 3D hydrogel constructs to an applied alternating electric field as a label-free non-destructive monitoring approach. The relationship between β -dispersion parameters (permittivity change - $\Delta \varepsilon$, cole-cole slope factor - α , critical polarization frequency - f_c) over the frequency spectrum and critical cellular quality attributes are investigated. Results show that alginate constructs containing a higher number of viable cells (human adipose derived stem cells - hASC and osteosarcoma cell line - MG63) were characterized by significantly higher $\Delta \varepsilon$ and α (both p < 0.05). When extended to bioprinting, results showed that changes in hASC proliferation and viability in response to changes in critical bioprinting parameters (extrusion pressure, temperature, processing time) significantly affected $\Delta \varepsilon$, α , and f_c . We also demonstrated monitoring of hASC distribution after bioprinting and changes in proliferation over time across the cross-section of a bioprinted medial knee meniscus construct. The trends in $\Delta \varepsilon$ over time were in agreement with the alamarBlue assay results for the whole construct, but this measurement approach provided a localized readout on the status of encapsulated cells. The findings of this study support the use of dielectric impedance spectroscopy as a label-free and non-destructive method to characterize the critical quality attributes of bioprinted constructs.

Keywords: PAT; Bioprinting process parameters; biofabrication process monitoring; quality assessment;

1.0 Introduction

Advances in biofabrication science and technology are enabling the fabrication of living constructs with complex heterogeneous geometries with increased functionality and fidelity [1–3]. To help accelerate the scale-up/scale-out translation of biofabrication processes and engineered tissue technologies to production scale processes, current process development efforts must be complemented with the development of better quality monitoring tools. Real-time and non-destructive monitoring modalities can enhance biofabrication process control and performance validation driving further innovation in cellular and tissue constructs. Such process control tools enable a stronger emphasis of the link between the tissue construct design and process development to ensure effective control of all critical quality attributes (CQA). In-process measurement tools help monitor the state of the biofabricated process and assist in active control the process to maintain a desired state. Biofabrication processes must accommodate the sensing of the raw input materials – both living and non-living components, enhance the reliability of measurement tools to measure critical attributes, preferably in real-time, and ensure that all process end-points are met to ensure consistent quality of the output biofabricated product.

Examples of CQA end-points associated with living components of the biofabricated tissue constructs include the viable cell volume (VCV), distribution of encapsulated cells within the biofabricated construct and cellular state (e.g. differentiation potential of stem cells or assessing damage to cellular membranes) immediately post-fabrication. Other long-term end points include monitoring cellular proliferation rate within the construct and assessing cellular/tissue functional characteristics. Such end-points are significantly affected by biofabrication process parameters such as extrusion pressure, processing temperature, and processing time as well as bioreactor culture conditions for long term culture among other factors [4-8]. Currently the only method available to monitor constructs in real-time during biofabrication processes is via live video feed or by capturing optical images at regular intervals during the process [9,10]. Identified deviations are captured into a process model and process parameters are adjusted appropriately to help achieve desired dimensional characteristics. Although feature dimensions play an important role in the functionality characteristics of a biofabricated construct, it is equally essential that we monitor the living component of the construct – the cells, due to the inherent variability associated with biological components and its criticality to meeting the quality attributes of the construct design and functionality. Without the ability to assess or monitor the 'state' of the cellular component, all biofabrication processes will be limited in their translational ability, and it will not be possible to integrate them into a fully automated closed-loop controlled production system.

Currently, offline methods are used to assess the quality of bioprinted constructs, i.e. performed after the biofabrication process is completed. These methods primarily include histological and biochemical assays to evaluate viability and proliferation (e.g., LIVE/DEAD®, alamarBlue® L-Lactate®, MTT®), permeability (e.g., CultureCoat®, Caco-2), cell differentiation (e.g., Alizarin red staining), reproductive assays and morphological assays among others. These assays are fairly well established and standardized across literature. However, these methods are also slow and expensive to use and are primarily meant for 2D flat plate cultures. From a biofabrication perspective, the limitation in this approach is that it is inherently destructive; constructs have to be first fabricated, then stained and sectioned. Not only is it time consuming and labor intensive, but the biological characteristics of the construct including cell morphology and function can also be potentially altered during the sectioning and assaying process. These techniques cannot be used as real-time metrology tools to assess construct characteristics during the biofabrication process. New methods that are capable of evaluating the in-process state of cells and construct quality attributes are critical to the advancement of the manufacturing science of living biological systems.

There have been some recent efforts on the development of non-destructive quality assessment methods. For example, molecular probes have been investigated to detect biomarkers within the growing structures of cells or in the secreted extracellular matrix which can then be correlated with relevant CQA attributes [11,12]. Another recent example is the use of light-emitting fiberoptics within bioreactors to quantify cell density by measuring the amount of scattered light [13]. One mode of measuring key changes in the cellular constituents of a biofabricated construct is by assessing changes in the dielectric properties of the cells within the construct post-fabrication. Dielectric Impedance spectroscopy (DIS) involves recording relative permittivity resulting from the dielectric response of cells to an alternating electric field applied across a range of frequencies. Indeed the dielectric properties of various types of cells have been studied in the past. DIS has been primarily used to monitor biomass of cell cultures, particularly in the bioreactor-based culture of mammalian cells, bacteria and insect cells for the production of recombinant proteins and viral vectors [14,15]. It has also been utilized in large vats to monitor the yeast-based fermentation of beer and wine [16,17]. DIS has also been used in a few novel 3D applications such as in distinguishing temperature induced cell morphology changes in bioreactors [18] and identifying cancerous and healthy tissue [19].

In this paper, we investigate the label-free and non-destructive DIS which can offer distinct advantages in assessing quality of 3D constructs during and after biofabrication. First, we have characterized the relationship between the cellular attributes (cell number, cell viability) of cast 3D hydrogel constructs and the dielectric characteristics of the encapsulated cells using a biomass monitor probe. We studied these relationships primarily on constructs containing human adipose derived stem cells (hASC) and have also verified the dielectric response to the change in number of viable cells with constructs containing MG63. Further, we have evaluated the capability of the DIS system to identify process deviations in bioprinting parameters such as extrusion pressure, temperature and processing time. Finally, we also demonstrate the use of DIS in monitoring cell proliferation within a construct in culture and present an approach to localized readout on the CQA of the living components within the construct.

2.0 Dielectric Response of Cells to an Alternating Current (AC) Field

Dielectric property of a material refers to its permittivity and conductivity constants in the presence of an alternating electric field. This property applies to cells owing to their double shell structure with the cell membrane and enclosed cytoplasm. In the presence of an alternating electric field, the phospholipid bilayer cell membrane acts as an insulator facilitating intracellular and extracellular polarization between the conductive cytoplasm and external media. This leads to an accumulation of positive and negative charges across the membrane making the cell behave like a capacitor, with the permittivity dependent on the frequency of the alternating electric field [20]. This phenomenon is known as the Maxwell-Wagner effect [18,21]. Such interfacial polarization is not observed in non-viable cells which are often characterized by a ruptured membrane resulting from necrosis or apoptosis [22]. In general, non-viable cells, cell debris, gas bubbles and other media components together have a negligible contribution to the permittivity [23,24], particularly within the frequency range in which cells are polarized. This distinction in permittivity characteristics of viable cells and damaged cells can be utilized to characterize the CQA of biofabricated constructs.

When the relative permittivity of cells are measured across a spectrum of frequencies, three notable dispersions are generated. The α-dispersion occurs at low frequencies in which intracellular and extracellular ions have adequate time to accumulate across the cell membrane resulting in higher interfacial polarization [25]. In this frequency region, there is a lack of the appropriate dielectric sensitivity necessary for quality monitoring. On the other end of the spectrum, y-dispersion occurs wherein ions do not have enough time to polarize at the high frequencies resulting in low permittivity readings [26]. This region is indicative of the permittivity of the media environment and is not suitable for quality monitoring. Between the α-dispersion where the cell membrane is highly polarized and y-dispersion where it is not, there is a steady decrease in permittivity with increasing frequency. This region of interest, usually characterized by an inverse sigmoid shape, is referred to as the β -dispersion. The β -dispersion is characterized by three important parameters – delta permittivity ($\Delta \varepsilon$), critical frequency (f_c) and cole-cole alpha (α). The difference between the permittivity in the high permittivity-low frequency region and low permittivity-high frequency region of the β -dispersion is referred to as the $\Delta \varepsilon$. The $\Delta \varepsilon$ is proportional to the total volume of viable cells as well as the mean radius of the cells present in the measurement volume (Equation 1) [27].

$$\Delta \varepsilon = \frac{9 \cdot P \cdot r \cdot C_m}{4\varepsilon_0} \tag{1}$$

Where P is the volumetric fraction of viable cells (i.e., volume of material bounded by the cell membrane per unit measurement volume), r is the radius of nominally spherical cells, C_m is the cell membrane capacitance per unit area, and ε_0 is the permittivity of free space (8.854 x 10⁻¹² F/m). The frequency corresponding to the midpoint of the β -dispersion slope is referred to as the critical frequency (f_c) [18,28]. The f_c is is inversely proportional to the mean cell radius (Equation 2) and is expected to be characteristic of a given cell type regardless of the total viable cell volume [29,30].

$$f_C = \frac{1}{2\pi \cdot r \cdot C_m(\frac{1}{\sigma_i'} + \frac{1}{2\sigma_0'})}$$
 (2)

Where σ_i' is the internal cytoplasmic conductivity of the cell and σ_0' is extracellular conductivity. \mathcal{C}_m , σ_i' , and σ_0' are constants for a given cell type. The slope of the β -dispersion is referred to as the Cole-cole α . The dimensionless α corresponds to τ (relaxation time) and the number of dipoles formed during the interfacial polarization across the cell membrane and has been shown to be related to cell size distribution within the measured volume [18,31].

3.0 Materials and Methods

We first computationally verified the dielectric response of cells (hASC) encapsulated within alginate constructs to an applied alternating electric field, and then experimentally characterized the relationship between DIS parameters and CQA attributes of 3D constructs under different scenarios via five separate studies. An overview of the experimental studies is presented in Figure 1. In the first two studies, we have mapped DIS parameters in response to the changes in the number of cells (Study 1) and % viability (Study 2) of hASC encapsulated in cast alginate 3D constructs. In the latter three studies, we have investigated how changes in 3D-bioprinting parameters affect the impedance spectral parameters in response to underlying changes in CQA of bioprinted constructs. In particular, the effect of non-optimal 3D-bioprinting parameters (high extrusion pressure and high print-head temperature) on the frequency response of encapsulated cells is characterized in Study 3. The effect of 3D-bioprinting processing time on the hASC encapsulated within alginate inside the print-head and the resulting DIS parameters from constructs bioprinted over time is assessed in Study 4. Finally, in Study 5, we have demonstrated a potential application of DIS to monitor cell proliferation in a 3D bioprinted knee meniscus construct in culture.

3.1 Simulation of Dielectric Response of Cells in 3D Hydrogels

A simplified 2D multiphysics simulation (AC/DC Module, COMSOL, Stockholm, Sweden) was created to verify the dielectric response of hASC encapsulated within alginate constructs. A cross-section of the simulation setup in the YZ plane is presented in Figure **2(a)**. The electric signals were applied to platinum electrodes which were modeled as rectangles with their dimensions and position reflecting those of the actual DIS probe used in the later experimental studies. Each cell was designed as two concentric circles (outer \emptyset = 22 μ m and inner \emptyset = 21.9 μ m) to capture the double shell properties of hASC, and a total of 1500 cells were encapsulated within the construct. The electrodes and the cellular construct were enclosed within a rectangular envelope that served as the volume containing Hank's balanced salt solution (HBSS) to reflect later experimental set up. Permittivity and conductivity of all entities in the model were assigned values as published in literature [35]. An electric field was generated by sending 1 μ A of current through the electrodes swept with frequencies between 50 - 20,000 kHz, and the permittivity of the model at those frequencies were obtained.

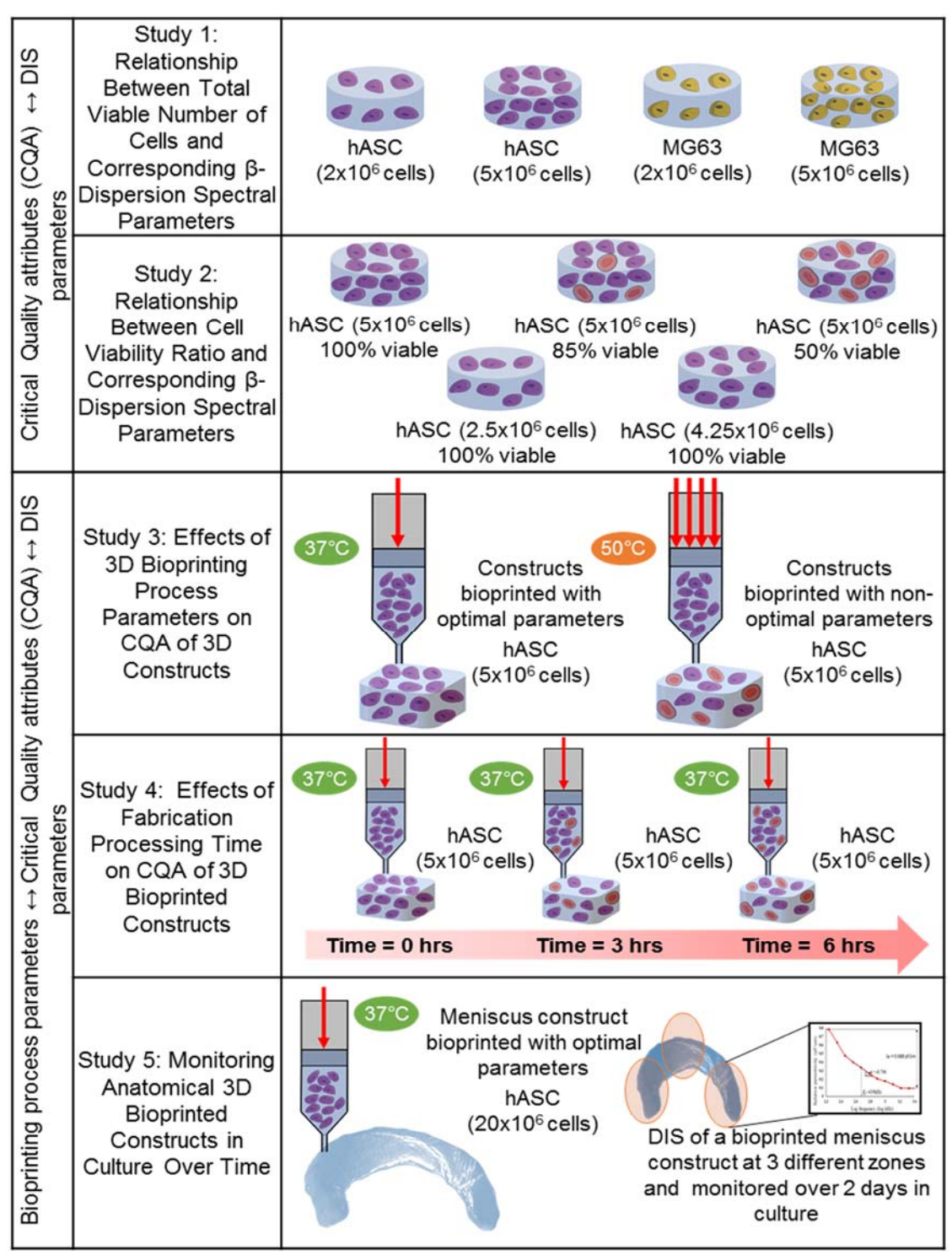


Figure 1. Overview of the five experimental studies

Figure **2(b)** and **2(c)** show the electric flux lines and the permittivity spectra after the alginate construct was introduced without and with 1500 cells, respectively. It can be observed that the pattern of electric field was altered and dispersion observed only in the presence of a cellular construct. This indicates that other entities in the model did not contribute to the permittivity dispersion at the measured frequency range. In the magnified image in Figure **2(c)**, it can be seen

that the electric field lines passed through the construct and through some cells. This phenomenon is the result of the higher conductivity of the cell cytoplasm relative to HBSS. We also observed a trend of increasing α and $\Delta\varepsilon$ with an increase in the number of encapsulated cells. The observations from this preliminary 2D computational model in the context of evaluating 3D cellular constructs are in agreement with the Maxwell-Wagner effect and the theory of polarization discussed in Section 2.0.

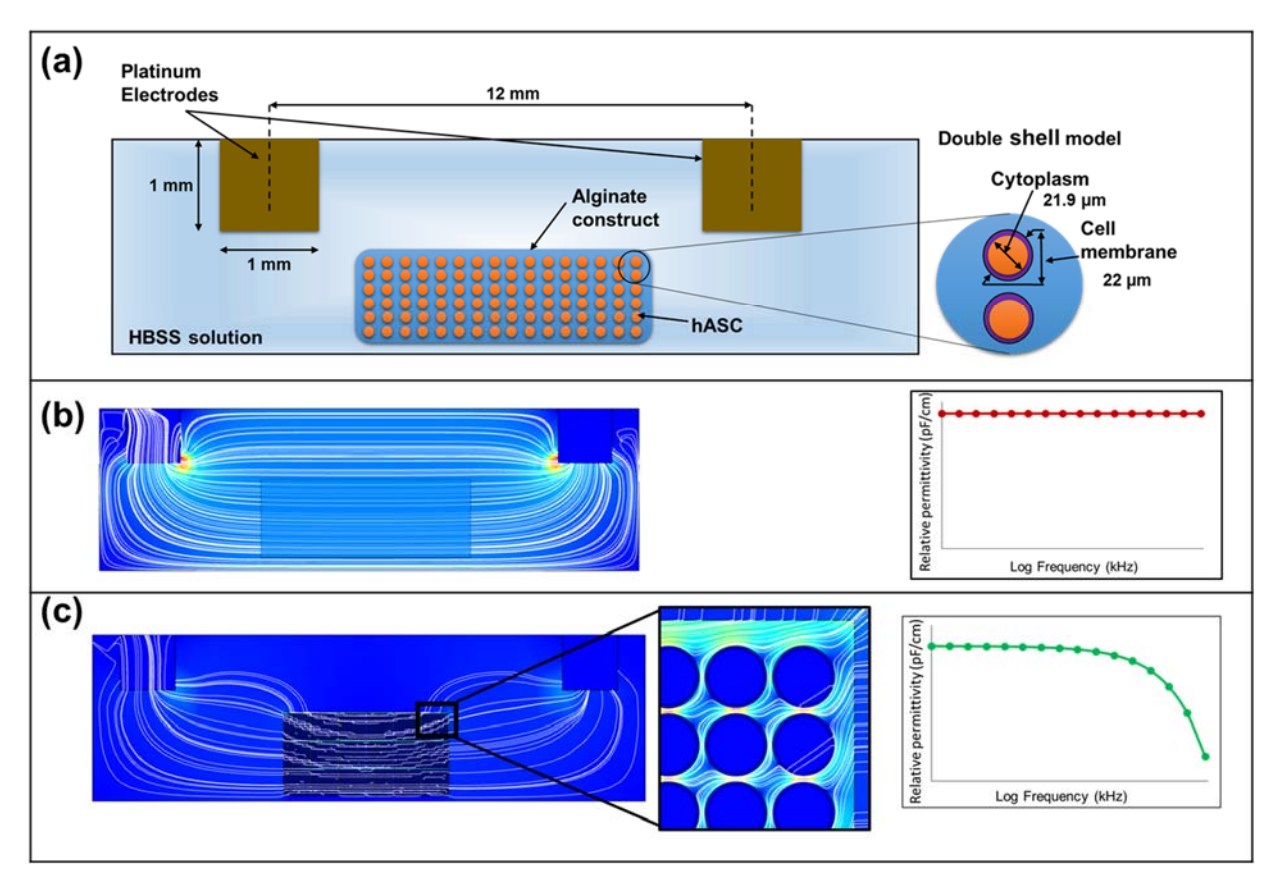


Figure 2. Simulation of Frequency Response of Encapsulated Cells in 3D Hydrogel Constructs. (a) Simulation model geometry with an alginate construct containing hASC. Center rectangle simulates a 400µm x 150µm thick alginate strand (b) Simulated electric field lines in the presence of alginate construct without hASC and the permittivity response to the change in frequency (c) Simulated electric field lines in the presence of alginate construct with 1500 hASC and the permittivity response to the change in frequency

3.2 Cell Expansion

Human ASC (StemPro® R7788115, Thermo Fisher Scientific, Waltham, MA) were the primary cell type used in all five studies in this paper. The hASC were cultured with MesenPro RS basal medium containing growth supplement (Thermo Fisher Scientific) and 1% L-Glutamine (Thermo Fisher Scientific) in a Corning® CellBIND® Surface HYPERFlask® (10-layer, 1720 cm² surface area; Corning, NY) at 37°C (5% CO₂). The flask was primed with 560mL of media and cultured up until a cell confluency of 80% was achieved. The cells were harvested by adding 60 mL of 0.25% trypsin EDTA (Thermo Fisher Scientific) after two washes with 100 mL of phosphate-buffered saline (PBS). The trypsinised cell suspension was neutralized with media and centrifuged to obtain cell pellets. In addition to hASC, MG63 cells (ATCC® CRL-1427, Manassas, VA) were also used in Study 1 to verify if the observed trends in DIS characteristics of 3D constructs containing hASC also extended to other cell types. The MG63 were cultured in Eagle's

Minimum Essential Medium (EMEM, no Ca, no Mg; ATCC) containing 10% v/v heat-inactivated fetal bovine serum (FBS; Thermo Fisher Scientific) in 75cm² cell culture flasks at 37°C (5% CO₂) and expanded with established protocols.

3.3 Bioink Preparation

Batches of $30\text{mL}\ 2\%$ w/v alginate solution were prepared by mixing 0.6g of sterilized sodium alginate powder (WillPowder, Miami Beach, FL) with 29.4mL of sterilized PBS and sonicated in an ultrasonic water bath at 60Hz for 2 hours [32]. The cell-encapsulated bioinks were prepared in a 15mL tube by mixing cell pellets with this 2% alginate solution in appropriate proportions required for each study. For Study 1, cell pellets of MG63 (2 x 10^6 and 5 x 10^6 cells) and hASC (2 x 10^6 and 5 x 10^6 cells) were suspended in 0.5mL of 2% alginate solution to prepare the four bioink groups. For Study 2, the bioinks were prepared with varying combinations of hASC number and % cell viability as shown in Table 1. For bioinks with 50% and 85% cell viabilities (groups B and D, respectively), the appropriate proportion of cells were rendered non-viable through heat inactivation before mixing with alginate solution. The bioink for Studies 3 and 4 was prepared by suspending 5 x 10^6 hASC in 2mL of 2% alginate solution. 20 x 10^6 hASC were suspended in 5mL of 2% alginate solution for the bioink in Study 5.

Table 1. Bioink formulations with varying number of hASC and cell viability for Study 2

	Total number of hASC	Number of viable hASC	Corresponding cell viability
Group A	5 x 10 ⁶	5 x 10 ⁶	100%
Group B	5 x 10 ⁶	2.5 x 10 ⁶	50%
Group C	2.5 x 10 ⁶	2.5 x 10 ⁶	100%
Group D	5 x 10 ⁶	4.25 x 10 ⁶	85%
Group E	4.25 x 10 ⁶	4.25 x 10 ⁶	100%

3.4 Casting of 3D Cellular Constructs

The 3D constructs required for Studies 1 and 2 were fabricated by casting 500μ L bioink in wells of 24-well and 12-well culture plates, respectively. The bioink was then crosslinked with 500μ L of 2% CaCl₂ for 5 minutes resulting in Ø12 X 5 mm thick constructs for Study 1 (n = 3 per group) and Ø18 X 3 mm thick constructs (n = 3 per group) for Study 2. The constructs were then immersed in wells containing 1mL of 2% CaCl₂ to improve their degree of crosslinking and strength. Finally, these constructs were washed in wells containing 1mL of deionized (DI) water prior to DIS evaluation.

3.5 3D Bioprinting of Cellular Constructs

For Study 3, cuboids of 20 x 20 x 3 mm were 3D-bioprinted with optimal and non-optimal parameters (Table 2; n = 3 per group) to obtain ideal (i.e., high cell viability) and non-ideal (i.e., low cell viability) constructs, respectively. The cuboid was modeled as a STL file in MagicsRP (Materialise NV, Leuven, Belgium) and sliced with appropriate layer height in using BioplotterRP (EnvisionTEC, Gladbeck, Germany). The sliced file was processed in Visual Machines (EnvisionTEC) and appropriate set of bioprinting process parameters (Table 2) were assigned. 2mL of cell-encapsulated bioink was filled into the stainless steel cartridge and bioprinted on a 3D-Bioplotter (Manufacturer series, EnvisionTEC). Each layer of the bioprinted construct was partially crosslinked by micro-pipetting sterile 1% CaCl₂ solution over the printed construct. The entire 2mL bioink was bioprinted to complete each ideal and non-ideal construct. Post printing, each construct was immersed in a 3mL of 2% CaCl₂ in a well of a 6-well plate for 5 minutes to improve the degree of crosslinking. Finally, the constructs were washed in wells containing 3mL of DI water prior to DIS evaluation.

Table 2. 3D Bioprinting Process Parameters for Fabricating Ideal and Non-ideal Constructs for Studies 3 and 4

	Non-optimal Parameters (Study 3)	Optimal Parameters (Studies 3 and 4)
Total number of hASC	5 x 10 ⁶	5 x 10 ⁶
Nozzle diameter	0.2 mm	0.3 mm
Extrusion pressure	0.12 N/mm ²	0.03 N/mm ²
Print-head temperature	50°C	37°C
Print-head speed	18 mm/sec	12 mm/sec
Laydown orientation	0°/ 90°	0°/ 90°
Needle height offset	0.5 mm	0.2 mm
Number of layers	2	3

For Study 4, the same 3D model (20 x 20 x 3 mm) was bioprinted using only the optimal parameters (Table 2) out of the entire 2mL of bioink containing 5 x 10^6 cells at 37° C. The first sample was bioprinted immediately (time 0), and the second and third samples were printed after 3 hours and 6 hours, respectively. Each sample was evaluated via DIS immediately after it was bioprinted and crosslinked.

To assess the cell viability through offline fluorescent labeling methods and to help compare spectral signal characteristics, all constructs were subjected to the LIVE/DEAD® assay (Life Technologies, Carlsbad, CA) following DIS measurements. Each construct was placed in 1mL PBS containing 0.5µl calcein AM and 2µl EthD-I and incubated for 10 minutes and imaged using a fluorescence microscope (Leica DM5500B, Leica Microsystems, Wetzlar, Germany). For each construct, images were obtained from five sections taken from five random locations. All images were binarized and quantified using "Analyze Particles" feature in ImageJ [33].

3.6 Digital Modeling and 3D Bioprinting of Knee Meniscus

3D model of a medial knee meniscus was constructed from MRI scan of the right knee joint of an unidentified patient. The MRI DICOM files were processed in Mimics Research (v18, Materialise NV, Belgium) to create a .STL file of the meniscus. The model was sliced with a layer height of 1 mm, and positioned on the platform using BioplotterRP. The file was then processed for bioprinting and assigned optimal process parameters (Table 2) in Visual Machines. Using the 3D-Bioplotter, 5mL of the bioink containing 20 x 10⁶ hASC was bioprinted following the meniscus STL geometry in a standard petri dish in a total of 6 layers, with 1% CaCl₂ solution micro-pipetted for crosslinking after every two layers. The completed construct was then immersed in 15 mL of 2% CaCl₂ solution for 10 minutes to improve the crosslinking. Finally, the construct was cultured (37°C, 5% CO₂) in a petri dish in 15mL of Mesenpro containing 10% alamarBlue (aB) reagent (Thermo Fisher Scientific) to assess hASC proliferation over 2 days, with the first reading taken 4 hours after bioprinting completion. Using the same procedure, 5 mL of acellular 2% alginate solution was bioprinted to serve as a control for the aB assay. Each media change for the cellular meniscus and acellular control contained 10% v/v of the aB reagent. At each time point, three 1mL samples were pipetted from each petri dish into a standard 24-well plate, and the absorbance was measured using a microplate reader (Tecan, Männedorf, Switzerland) with excitation and emission wavelengths of 570nm and 600nm, respectively. The absorbance data was converted to and is reported as % aB reduction.

3.7 Dielectric Impedance Spectroscopy (Relative Permittivity) Assessment

The dielectric permittivity spectra of the constructs were measured using a DIS flush probe (Ø25mm; ABER Instruments Ltd., Aberystwyth, UK) as illustrated in Figure 3. Test samples were exposed to the electric field established by the two sets of platinum electrodes on the bottom of the probe, and changes in electric field due to the capacitance of cells were amplified, processed and recorded as permittivity readings across the default frequency scan (50 – 20,000 kHz) using FUTURA SCADA (ABER Instruments Ltd., UK).

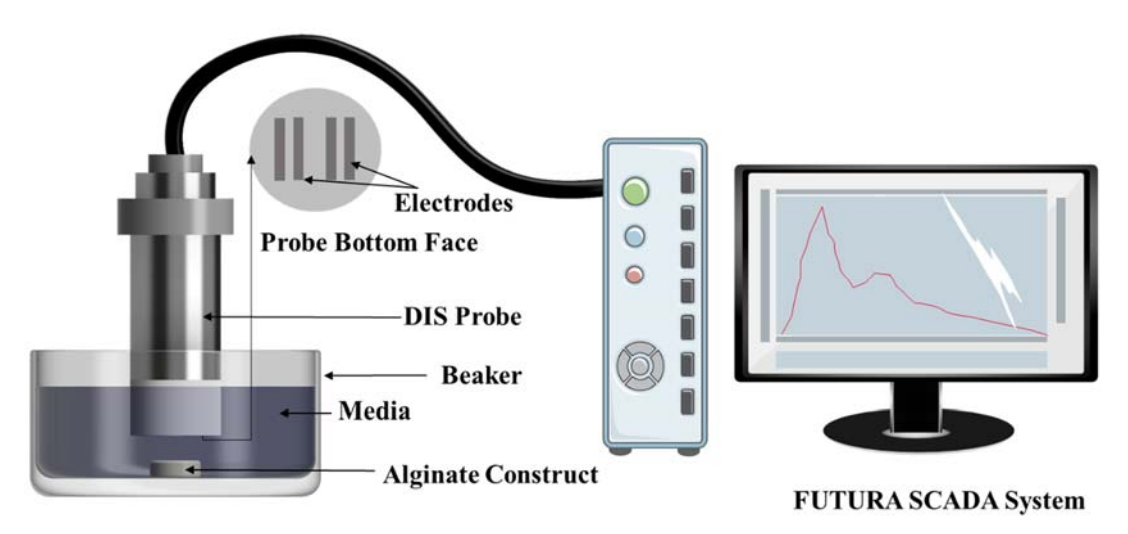


Figure 3. Measurement Setup for the Assessment of Relative Permittivity of Bioprinted 3D Constructs

During each experiment in Studies 1-4, the construct was gently placed underneath the probe (electrodes) inside a glass beaker (Pyrex, Corning, NY) containing 125mL of Hank's balanced salt solution (HBSS, Lonza, Walkersville, MD). For study 5, measurements were taken at three different locations along the meniscus construct. In each experiment, the total capacitance of the setup was measured and zeroed prior to introducing the construct. The measured capacitance was normalized using the probe constant to obtain the permittivity of the constructs.

A standard frequency scan of 50 - 20,000 kHz was performed on each construct, and data from the eleven preset frequencies between 150 - 2500 kHz (174, 224, 287, 368, 473, 607, 779, 1000, 1284, 1648 and 2115 kHz), as recommended for mammalian cell culture, was used for β -dispersion characterization [25,34]. β -dispersion curves of the constructs were created by plotting the relative permittivity against log scale frequency. The permittivity values at different frequencies are reported as an average of the permittivity readings over a 15-minute measurement interval. The $\Delta \varepsilon$, α , and fc values were determined from these β -dispersion curves. The $\Delta \varepsilon$ was calculated as the difference in relative permittivity between the low-frequency high-plateau and high-frequency low-plateau regions of the curve. The f_c was determined by fitting a fifth-degree polynomial to the decline region of the curve and solving for the frequency at a relative permittivity value of $\Delta \varepsilon/2$. The α was calculated as the slope of the decline region of the curve. Before conducting the five primary studies (Figure 1), experiments were performed to determine if the DIS evaluation method had an effect on the cell viability of the constructs. The results showed that the DIS measurement method itself did not affect the viable cellular volume in the constructs (See supplementary information-Figure S1).

3.8 Statistical Analysis

In Study 1, for each cell type, t-tests were performed to compare the β -dispersion parameters ($\Delta \varepsilon$ and α) between the two groups with different cell numbers ($\alpha = 0.05$, JMP Pro, Cary, NC). For

Study 2, one-way ANOVA and Tukey's HSD post hoc tests were performed on $\Delta \varepsilon$ and α with cell number-cell viability combination as the independent variable. For Study 3, one-way ANOVA and Tukey's HSD post hoc tests were performed on $\Delta \varepsilon$ and α with a given set of bioprinting parameters as the independent variable.

4.0 Results

4.1 Study 1: Determining Relationship Between Total Viable Number of Cells and Corresponding β -Dispersion Spectral Parameters

The β -dispersion curves of cast constructs containing hASC (2 x 10⁶ and 5 x 10⁶ cells, n = 3 per group) and the resulting DIS parameters ($\Delta \varepsilon$ and α) are presented in Figure **4**. Results show that constructs containing 5 x 10⁶ cells had a significantly higher $\Delta \varepsilon$ and α (p < 0.05) than constructs with 2 x 10⁶ cells. These experimental results are in agreement with theory wherein $\Delta \varepsilon$ is directly proportional to the total volume of viable cells present in the measurement volume (P, Equation **1**); higher number of cells in the construct implies higher viable cell volume. As a validation that these relationships between number of cells in the construct and $\Delta \varepsilon$ and α hold true across cell types, the same statistically significant relationships (p < 0.05) were reported in constructs containing MG63 (2 x 10⁶ and 5 x 10⁶ cells, n = 3 per group) as presented in Figure **5**. The results confirm the ability to detect changes in the number of cells by monitoring changes in α and $\Delta \varepsilon$.

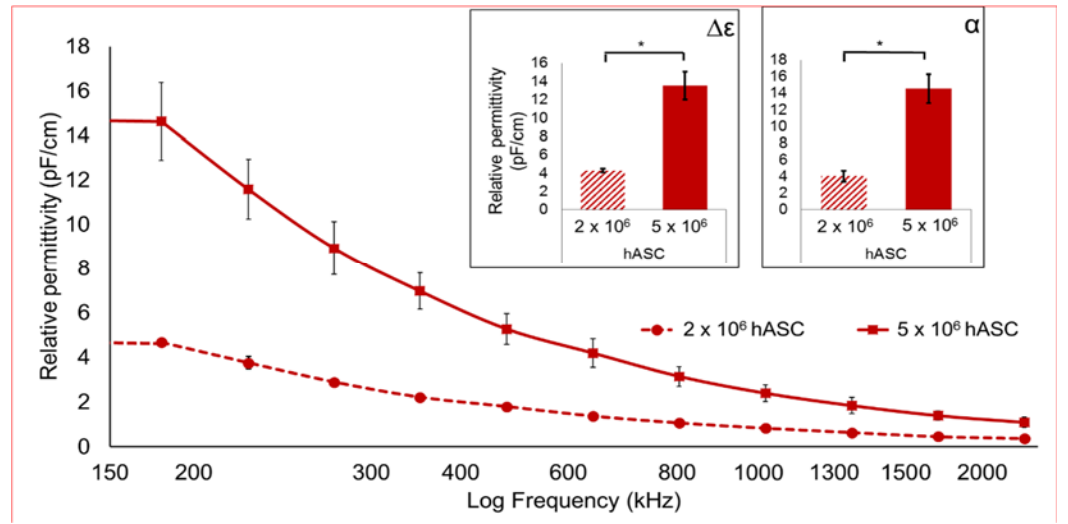


Figure 4. β-dispersion curve and characteristics of constructs with varying total number of hASC. Insert graphs presents values of the DIS parameters ($\Delta \varepsilon$ and α) of the constructs. * represents statistically significant difference (p < 0.05) between groups.

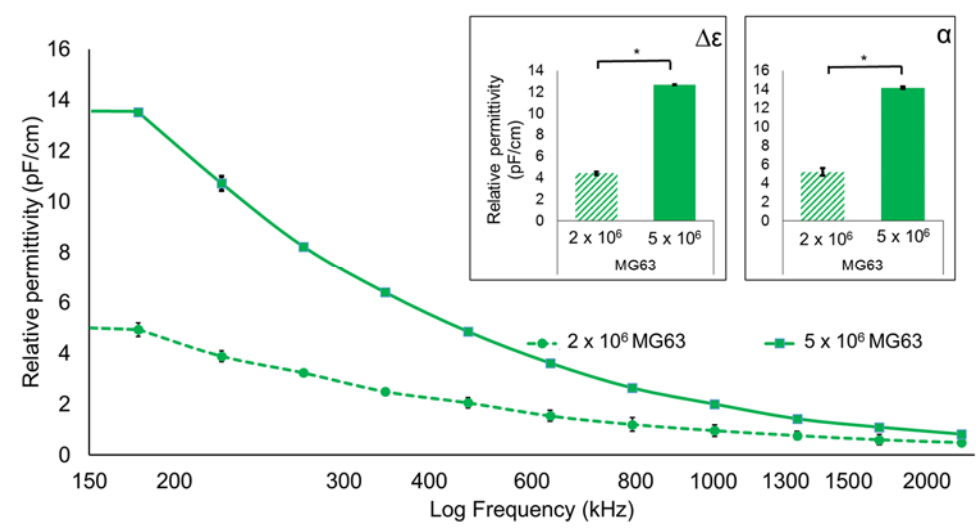
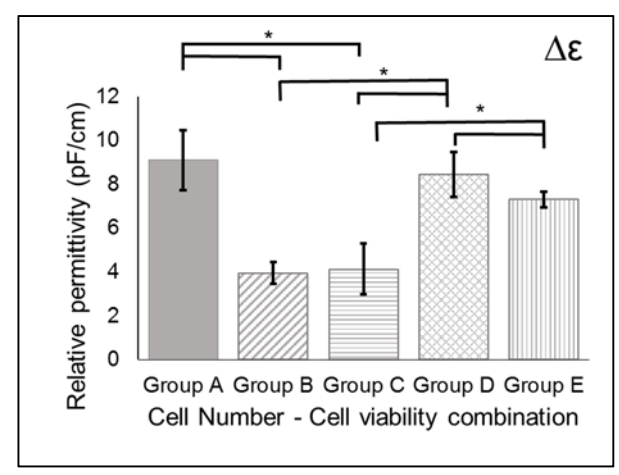


Figure 5. β-dispersion curve and characteristics of constructs with varying total number of MG63. Insert graphs presents values of the DIS parameters ($\Delta \varepsilon$ and α) of the constructs. * represents statistically significant difference (p < 0.05) between groups.

4.2 Study 2: Determining Relationship Between Cell Viability Ratio and Corresponding β -Dispersion Spectral Parameters

Five groups of cast constructs containing hASC (Table 1, n = 3 constructs per group), each with a different combination of cell number and cell viability, were subject to DIS evaluation. In theory, the characteristic DIS spectra result from the polarization of only healthy viable cells. Accordingly, these five combinations of cell number and cell viability were chosen to test the hypothesis that the permittivity $(\Delta \varepsilon)$ of constructs containing the same number of viable cells (and corresponding cell volumes, P, in Equation 1) are not statistically significantly different even when their %viability (resulting from a different total number of viable and non-viable cells) is different. Groups A and B contained the same total number of cells, but 100% of the cells in group were viable compared to only 50% viable cells in Group B. Similarly, Groups A and D contained the same total number of cells, but only 85% of cells in Group D were viable. In theory, $\Delta \varepsilon$ of Group A should be higher than those of Groups B and D, and Group B should have the lowest $\Delta \varepsilon$ among the three. In contrast. Groups B and C contained different total number of cells, but the total number of viable cells in both was the same. The same was true about Groups D and E which contained different total number of cells but the same number of viable cells. In theory, the $\Delta \varepsilon$ of each of Groups B and C and Groups D and E should not be significantly different. The β-dispersion plots and corresponding $\Delta \varepsilon$ and α of the five groups are presented in Figure 6.



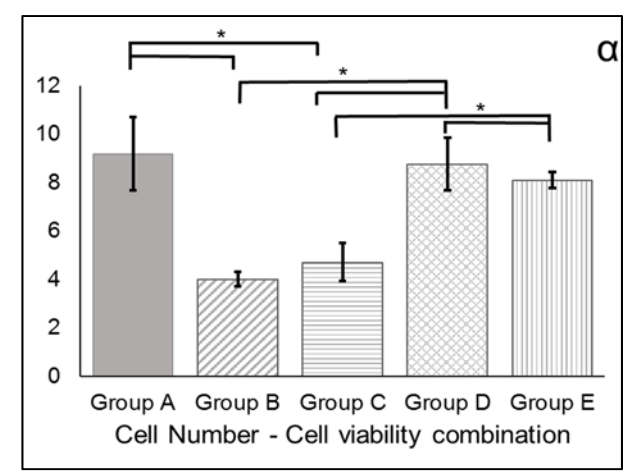


Figure 6. Comparison of β-dispersion parameters for constructs with varying hASC viabilities. * represents statistically significant difference (p < 0.05) between groups.

Results of one-way ANOVA show that the bioink group (cell number and cell viability combination) had a significant effect (p < 0.05) on both $\Delta\varepsilon$ and α . Individual comparisons of groups via Tukey's HSD post-hoc tests showed that $\Delta\varepsilon$ of Groups A and B as well as of Groups B and D were significantly different (p < 0.05), but those of Groups B and C as well as of Groups D and E were not. This result corresponds with the theoretical relationships that were discussed above and confirms the hypothesis that $\Delta\varepsilon$ depends only on the viable number of cells and not the total number of cells in the 3D construct. Although $\Delta\varepsilon$ of group A was 7% higher than that of Group D, the difference was not statistically significant. This lack of statistical significance can be attributed, in part, to the sensitivity of the probe in its current design and inherent variability associated with the manual fabrication and cell counting procedures used to make and assess the constructs. The critical frequency, f_c of the constructs were also evaluated and was not statistically significantly different between the groups. This observation corresponds to the theory that f_c of constructs remains the same for a given cell type irrespective of the volume of the viable cells.

These results confirm the ability to detect changes in $\Delta \varepsilon$ and α corresponding to underlying changes in cell viability, keeping in mind the resolution of the current DIS probe and system wherein differences in cell viability of 15% or less cannot be detected with statistical significance. Taken together, results of Studies 1 and 2 demonstrate the ability to non-destructively monitor the proliferation and viability of cells within maturing 3D constructs in culture by tracking $\Delta \varepsilon$ and α over time via DIS.

4.3 Study 3: Determining Effects of 3D Bioprinting Process Parameters on CQA of 3D Constructs

The effects of 3D bioprinting process parameters on cellular quality attributes have been studied, and it is known that variations in critical process parameters can adversely affect these attributes in bioprinted constructs [35,36]. Study 3 was designed as a simulated scenario to investigate effects on DIS parameters when the 3D bioprinting process was operated with or without optimal process parameters. From a practical perspective, the results would demonstrate whether monitoring DIS parameters of the bioprinted construct could help identify any process deviations from preset optimal conditions.

Representative Live/Dead images of the constructs (20 x 20 x 3 mm, 5 x 10^6 hASC) bioprinted with optimal and non-optimal process parameters (Table 2), are presented in Figure 7(a) and 7(b) respectively. The constructs in the optimal parameters group had higher cell viability (87 \pm 1%)

than constructs in the non-optimal parameters group ($50 \pm 1\%$). An example of the cell viability image analysis data across different sections of a construct bioprinted with optimal and non-optimal parameters is presented in supplementary information-Figure **S2**. These viability results are in accordance with extrusion-based bioprinting literature wherein increase in extrusion pressure has been demonstrated to adversely affect cell viability; viability dropped from 85% to 50% as the pressure was increased from 0.03 to 0.27N/mm² [35]. This decrease is attributed to irreversible cell injury caused by high pressure which leads to cell necrosis and apoptosis. For the non-optimal group in this study, primarily, the 0.12N/mm² extrusion pressure, which is above the recommended range of 0.01 - 0.10N/mm² [36] coupled with extrusion temperature of 50°C, which is higher than 37°C recommended for cells, would have caused significant irreversible cell injury leading to cell death and manifesting as lower % viability.

The DIS parameters and β -dispersion plots of the two groups are presented in Figure **7(c)** and **7(d)**, and correspond with the cell viability results of Live/Dead analysis. Unlike the plot of the optimal bioprinting parameters group, the plot of the non-optimal parameters group did not resemble the inverse sigmoid shape which is characteristic of a β -dispersion plot [14,30,37,38]. These discrepancies in cell viability between the two groups are also reflected in the DIS parameters (Figure **7(c)**); the $\Delta \varepsilon$, α , and f_c of constructs in the two groups were significantly different (p < 0.05). The $\Delta \varepsilon$ of the optimal group was 70% higher than those of the non-optimal group, and signifies the decrease in volume of viable cells in the measured volume as per Equation **1**. For the non-optimal group, the incongruous shape of the β -dispersion plot and the higher f_c compared to the optimal group is an indication of adverse changes in cell morphology during the bioprinting process [35,36,39]. From Equation **2**, it is known that f_c increases with decreasing cell radius, and it has been demonstrated that the shear stresses experienced by the cells at higher extrusion pressures compress the cells [35], which corroborate our findings here.

These results demonstrate the ability to use DIS monitoring to identify deviations in process parameters that would result in constructs with inferior cell quality attributes. We used extrusion bioprinting as a model process in this study, but the DIS monitoring method can be extended to other 3D biofabrication processes as well. For example, in laser-assisted bioprinting [40–42], cell viability has been shown to be affected by the kinetic forces experienced by the cells due to the laser-induced jet dynamics [41]. DIS can be used to monitor and map the effects of changing jet dynamics on the viability of cells in the bioink.

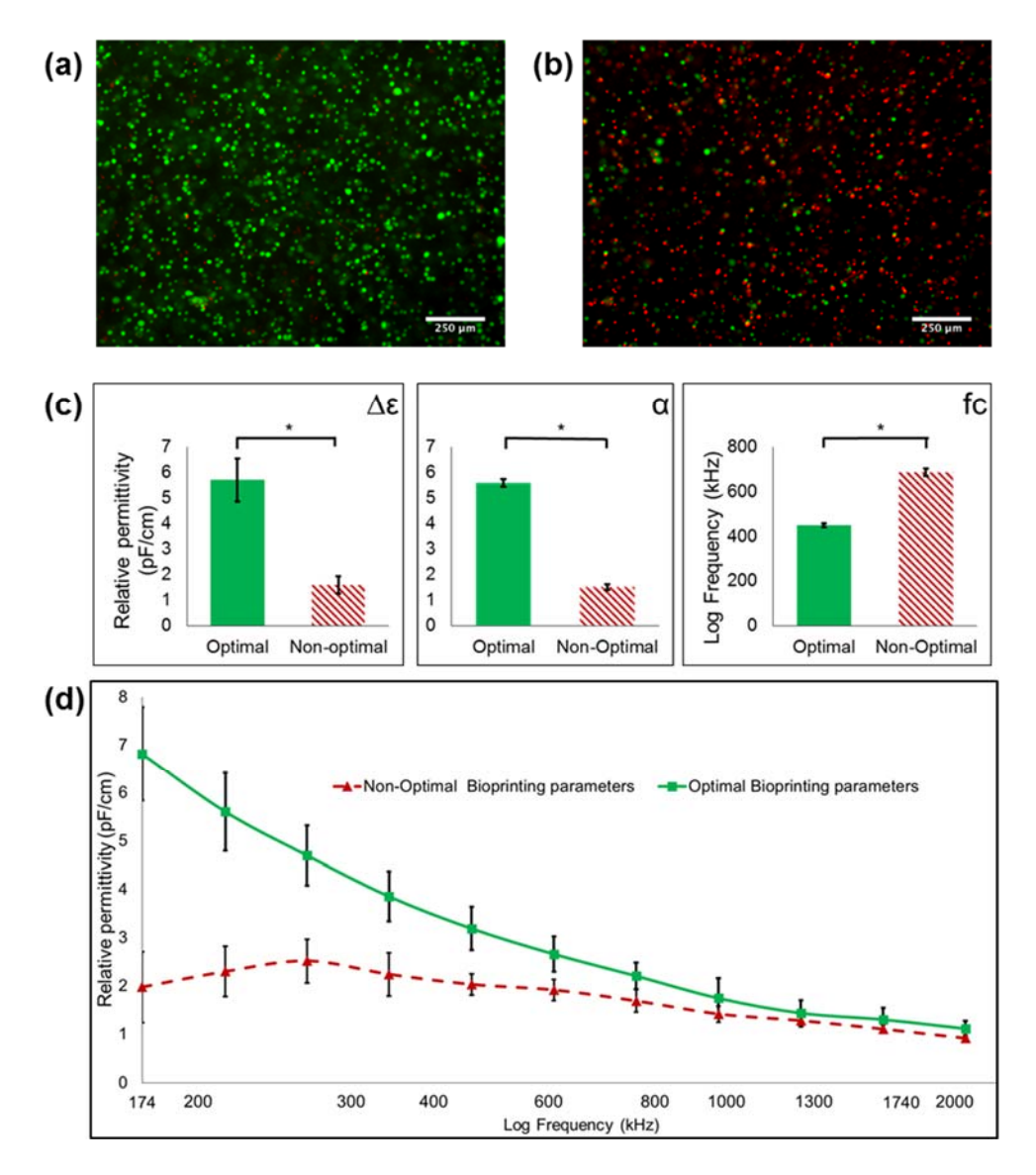


Figure 7. (a) Representative Live/Dead image of constructs bioprinted with optimal process parameters. (b) Live/Dead images with non-optimal process parameters. Scale bar is 250μm. (c) DIS parameters and (d) β-dispersion curve of 3D bioprinted constructs with optimal and non-optimal process parameters as given in Table 2. *represents statistically significant difference (p < 0.05) between groups. Note that the destructive Live/Dead assay was performed after completing DIS evaluations.

4.4 Study 4: Determining Effects of Fabrication Processing Time on CQA of 3D Bioprinted Constructs

One of the important factors to consider while 3D bioprinting is the time required for fabrication of the constructs [7,43]. This is especially relevant in extrusion-based processes which may require a substantial amount of time to dispense the bioink due to limitations with the extrusion flow rate compared to other processes. The flow rate, primarily controlled by the extrusion pressure during bioprinting, depends on the viscosity of the bioink and the flow and shear stresses that the cells can endure. The viscosity of bioinks must be the within a range that allows extrusion at lower pressures (less than 0.1N/mm²) [36] and enables the construct to maintain shape fidelity post-printing. Depending on the bioink properties, bioprinting process parameters, and size and geometry of the construct, the cells encapsulated in the bioinks may often remain stored in the

printing reservoir or cartridge for more than 2 hours [7,43]. The conditions in the reservoir may not be conducive to the bioactivity of the cells over longer time periods. For example, high cell concentration in the bioink can make the cells more prone to hypoxia and media deprivation within the limited nutrient volume of the material reservoir.

In this study, we evaluated if any changes in cell viability due to long processing times can be captured using DIS. Constructs were bioprinted immediately after loading the 3D-Bioplotter cartridge or after 3 hour or 6 hour intervals with the bioink stored in the cartridge at 37°C. Results of Live/Dead assay showed the hASC viability to be 90%, 70%, and 64% after intervals of 0 hours, 3 hours, and 6 hours, respectively. The cell viability image analysis data across different sections of the constructs bioprinted at different time intervals is presented in supplementary information-Figure **S3**. The β -dispersion plots and DIS parameters from the three constructs are presented in Figure **8**. The β -dispersion plots of all three constructs followed the inverse sigmoid shape, and corresponding to the Live/Dead results, $\Delta \epsilon$ and α decreased with increasing process intervals, signifying a decrease in volume of viable cells (Equation **1**). These results further demonstrate the ability of the measurement approach to conduct quality assessment of the bioprinted constructs.

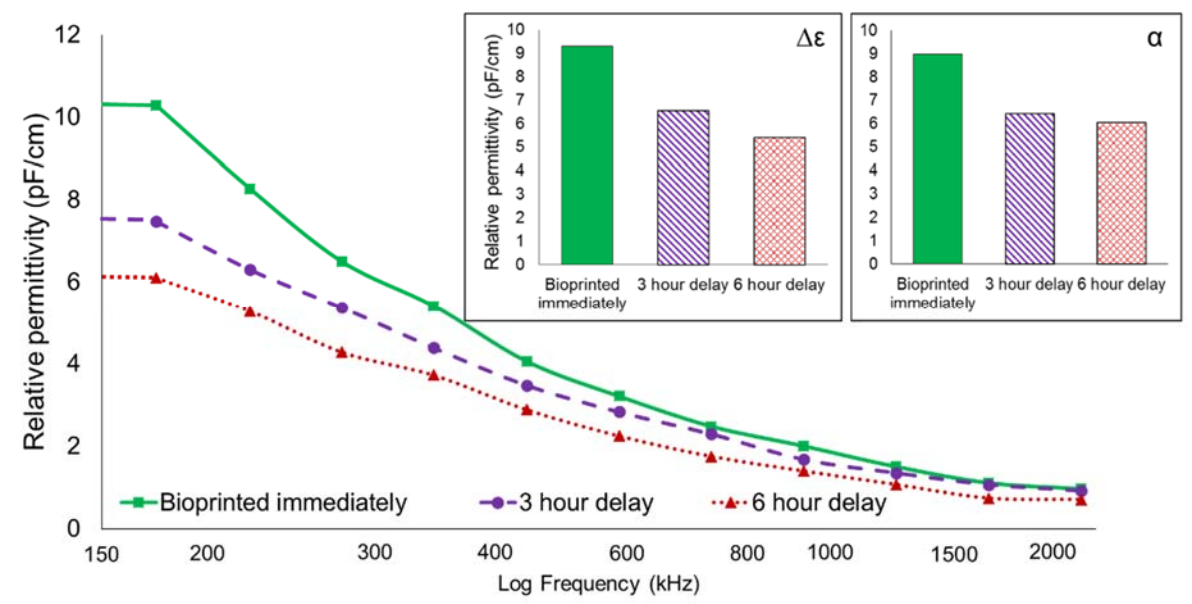


Figure 8. β -dispersion curves of bioprinted constructs evaluated immediately and after 3 hour and 6 hour delay.

4.5 Study 5: Monitoring Anatomical 3D Bioprinted Constructs in Culture Over Time

In Study 5, we investigated the ability to use DIS to monitor the changes in cellular attributes in an anatomically relevant human medial knee meniscus construct. To capture any variations in initial hASC distribution and track changes in hASC proliferation over time along the crescent-shaped geometry, DIS measurements were taken at three different zones of the construct immediately after bioprinting and after 24 hours and 48 hours in culture. Localized variations in cell distribution and cell viability in constructs without vascular networks due to proximity of different regions to the culture media, poor nutrient diffusion and hypoxia have been reported in literature [6,7,44,45]. Cell clustering and agglomerations caused during bioink preparation and the bioprinting process itself also contribute to such localized variations which we intended to capture using DIS.

The bioprinted medial meniscus construct and DIS evaluation setup are shown in Figure **9**. The % aB reduction measured for the entire construct and $\Delta \varepsilon$, which is proportional to the viable cell volume, obtained from β -dispersion curves of each of the three zones, are plotted in Figure **9** (e). The aB results indicate an increase in proliferation from day 1 to day 2 and a drop from day 2 to day 3. The same trend was observed in $\Delta \varepsilon$ consistently across the three zones. Furthermore, at each time point, the trend in $\Delta \varepsilon$ across the zones was the same, with the highest $\Delta \varepsilon$ reported in zone 2 and the lowest $\Delta \varepsilon$ in zone 3, indicating localized variations in cell distribution. That the trend in $\Delta \varepsilon$ across the zones was the same also indicates that all regions of constructs were equally affected by cell culture conditions. The correlation between % aB reduction and $\Delta \varepsilon$ demonstrates that DIS can be used to monitor the cellular quality attributes of 3D bioprinted constructs in culture. The biggest advantage of DIS here is that the quality attributes can be measured non-destructively over time (unlike sectioning in Live/Dead assay), and more granularly across multiple regions of 3D constructs relatively quickly (unlike aB assay wherein only a single reading can be obtained for an entire construct irrespective of its size and geometric complexity).

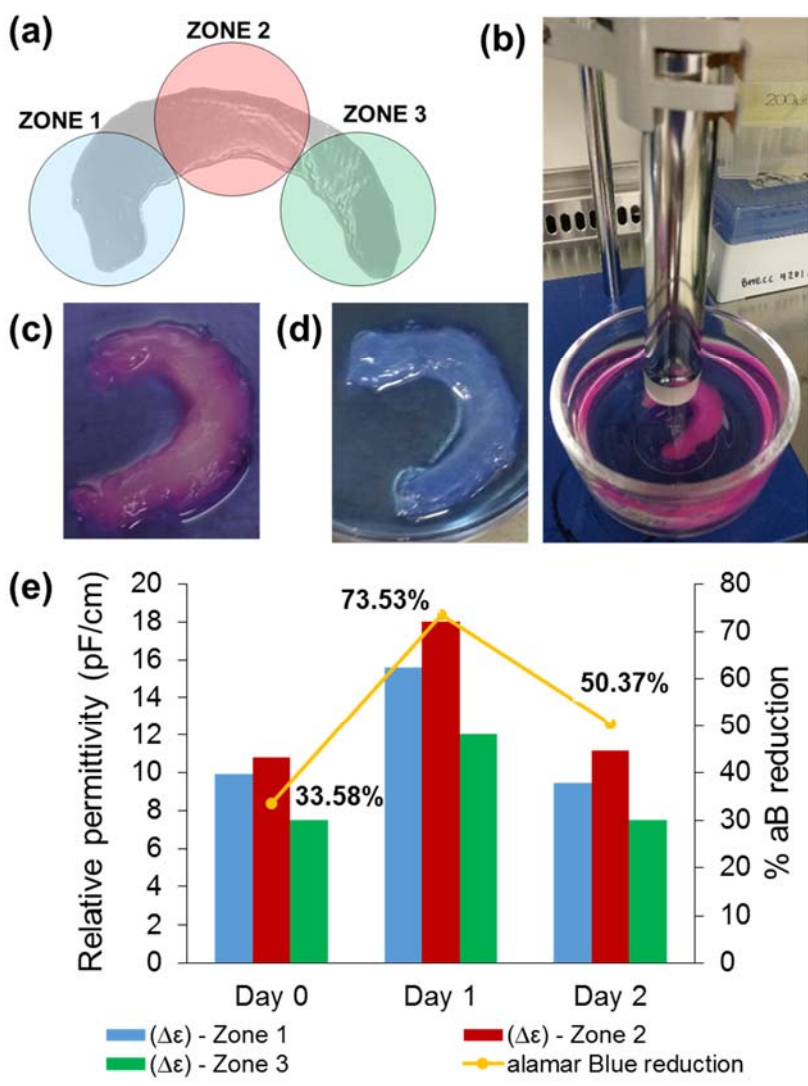


Figure. 9 (a) Schematic of the zones of DIS measurement of the bioprinted meniscus construct. **(b)** DIS evaluation of 3D bioprinted meniscus at zone 1. **(c)** 3D bioprinted meniscus containing 20 x 10^6 hASC **(d)** 3D bioprinted meniscus construct without cells used for alamarBlue control **(e)** $\Delta\epsilon$ of different zones of meniscus over 2 days and % aB reduction of the meniscus construct.

5.0 Discussion

There have been several recent efforts on the development of non-destructive monitoring methods for 2D and 3D cell cultures. These methods are based on principles such as optical refraction, chemical affinity and electrical impedance. In the latter, electrical properties of cells have been utilized to draw inferences about the cell quality attributes. Most recently, Canali et al. utilized the principle of electric cell-substrate impedance sensing (ECIS) to monitor proliferation of 3D cell cultures over time [46]. Their measurement set up consisted of electrodes along the four vertical walls of the culture chamber. Lee et al. used a DIS system with four pairs of electrodes to monitor cell proliferation, cell migration and drug-induced cell death overtime in a 3D culture chamber [47]. With electrodes that are fixed at a spot, this approach works well for long term monitoring of cultures where the total measurement volume does not change significantly over time, but it may not be suitable in 3D bioprinting where the constructs are built up layer by layer. The electric field strength would have to be constantly increased to account for the increase in construct volume with each bioprinted layer. This becomes problematic especially for large constructs with anatomical 3D geometry. In addition, the fixed electrodes approach [46, 47] also lacks the flexibility in gathering impedance data from localized regions along the constructs' X-Y cross-sections. As such, this paper represents the first known measurement approach suitable for non-destructively characterizing the critical quality attributes of 3D bioprinted constructs. The primary advantages of the DIS probe-based measurement approach include its ability to selectively assess specific regions of the 3D construct, and its potential of being integrated directly on to the bioprinter print-head.

The studies in this paper taken together have demonstrated how DIS can be used to non-destructively evaluate cell proliferation and cell viability in 3D constructs, and an approach to extending the measurement approach to monitor changes in constructs in culture over time. In theory, it may be possible to use DIS to track changes in cell morphologies, particularly cellular aggregation and cellular state changes. Monitoring changes in the dielectric properties of the cells is only complete when reading both resistance and capacitance signals, essential components of encapsulated cells impeding the flow of AC current when placed in an electric field. This particular study focused on the capacitance (hence relative permittivity) of the encapsulated cells within the construct. In future, monitoring both resistance and capacitance as individual signals would provide better insight into the cell-cell barrier resistance when cellular spheroids form within the construct and to measure the overall impedance characteristics of the printed 3D construct. This probe-based DIS system and measurement approach also has the potential to be integrated with a 3D bioprinting gantry system enabling in-process quality evaluation during bioprinting.

Several tissue engineering and regenerative medicine applications use stem cells that are induced to differentiate into application-specific cell types as the construct matures in culture [44,48,49]. In such applications, DIS parameters can be potentially used to detect differentiation state of the cells. While an increase in $\Delta \varepsilon$ over time indicates cellular proliferation, a change in f_c without a corresponding change in $\Delta \varepsilon$ will indicate underlying changes in physiological state of cells such as those observed during stem cell differentiation. Deduction of the cellular physiological state including stem cell differentiation based on β -dispersion characteristics, albeit in monolayer cultures, has been reported in literature [50,51]. Such investigations in the context of 3D bioprinted constructs will be a part of our future work. These experimental studies can be complemented by computational modeling. The preliminary 2D model discussed in section 3.1 can be extended to 3D and further refined by more detailed modeling of the DIS electrical circuitry and effective material properties to more closely reflect the experimental conditions.

The DIS probe used in this study was designed for use in large bioreactors and fermenters used in brewing industries [14,16,17,29]. The number of cells in suspension in these applications

typically exceeds 100 x 106, and the existing probe design and DIS system resolution has been optimized to account for such large cell numbers. The inability to distinguish between constructs with small differences in the total volume of viable cells as reported in Study 2 resulted, in part, from these sensitivity and resolution issues. In future, the DIS probe and system design will need to be optimized specific to 3D constructs. The following two approaches can be investigated to achieve this. First, the distance between the measurement electrodes at the bottom surface of the probe can be reduced. In the present design, the measurement volume encompasses a sphere of Ø40 mm underneath the probe. This measurement volume is dictated by the distance between the electrodes. Reducing the distance between the electrodes will make the measurement volume smaller enabling more precise localized CQA measurements over a 3D construct. Second, the resolution of the β-dispersion curves can be improved by increasing the number of frequencies at which the permittivity is measured within the 150 - 2500 kHz frequency range that is relevant to mammalian cells. At present, a frequency scan lasts for 30 seconds, permittivity readings are obtained across 25 discrete frequencies between a range of 50 - 20,000 kHz, and only eleven frequencies are relevant. In addition to a more focused scan range, increasing the number of measurement frequencies within the range (from the current eleven) can help improve the β-dispersion curve resolution. During the production scale fabrication of engineered tissue constructs, only one particular frequency may be needed to guery the CQA of the bioprinted construct. This is assuming that prior studies have been conducted to determine the appropriate frequency at which the CQA must be measured. Similar studies have been conducted in biopharmaceutical production and the selection of the frequency is highly dependent on the cell types involved [23,52]. Together, these changes can make the system more robust for quality monitoring of 3D bioprinted constructs

Although we demonstrated the evaluation of cast and extrusion-based 3D bioprinted constructs. DIS monitoring methodology itself is independent of the biofabrication process. This measurement approach can be easily extended to evaluate constructs made by other processes including vat polymerization [53,54], laser-assisted Bioprinting[40,41], inkjet bioprinting [49,55] among others. For layer-by-layer biofabrication process, DIS can be used for in-process monitoring wherein cellular quality attributes of each layer are measured and qualified immediately after a layer or a portion of it is printed. If the DIS parameters and corresponding underlying cellular attributes are deemed to be within pre-defined control limits, the process can continue onto the next layer. If the attributes in a particular layer are outside acceptable control limits, the process can be terminated. In the absence of such real-time process monitoring methods, significant effort and resources would have to be expended on creating and culturing a defective construct that would eventually be rejected in downstream manufacturing operations. Another potential approach in the latter situation would be to track the β-dispersion parameters during the fabrication process and then make in-process fabrication control parameter adjustments (such as pressure, temperature etc.) to keep CQA within control limits. To enable this, the relationship between superimposition and attenuation of electrical signals with addition of layers must be understood. We plan to investigate these aspects in our future studies.

6.0 Conclusion

In this study, we measured the ability of encapsulated cells in 3D bioprinted hydrogel constructs to polarize in the presence of an alternating current at different frequencies using dielectric impedance spectroscopy. We experimentally characterized the relationship between β -dispersion parameters and CQA of 3D constructs under various scenarios. In the first two studies, we mapped DIS parameters in response to the changes in the number of cells and % viability of hASC encapsulated in cast alginate 3D constructs. In the latter three studies, we investigated how changes in 3D bioprinting parameters affect the DIS parameters in response to underlying changes in CQA attributes of bioprinted constructs. In particular, the effect of non-optimal 3D

bioprinting parameters (high extrusion pressure and high print-head temperature) on β -dispersion parameters (change in permittivity $\Delta\epsilon$, critical frequency, f_c and the Cole-Cole parameter, α) was characterized in Study 3. The effect of 3D-bioprinting processing time on the hASC encapsulated within un-crosslinked sodium alginate inside the print-head and the resulting β -dispersion parameters from constructs bioprinted over time was assessed in Study 4. Finally, in Study 5, we demonstrated a potential application of DIS to monitor cell proliferation in a 3D bioprinted knee meniscus construct. Overall, DIS can be used as a label free, non-destructive method to evaluate critical quality attributes of biofabricated constructs, a necessary step to translating biofabrication processes to the production floor. Future work will involve integrating the measurement approach with the bioprinter to enable a real-time characterization of the biofabricated constructs.

7.0 Acknowledgement

The authors would like to gratefully acknowledge the support from the US NSF #1562139 and funds from the Comparative Medicine Institute. We also would like to thank Dr. Aditya Bhat, Director of Technology, Aber Instruments, UK, for providing us with technical guidance and access to the internal data logs of the ABER probe.

8.0 References

- [1] Starly B, Shirwaiker R, Leong K W, Starly B and Shirwaiker R 2015 3D Bioprinting Techniques 3D Bioprinting and Nanotechnology in Tissue Engineering and Regenerative Medicine (Elsevier) pp 57–77
- [2] Malda J, Visser J, Melchels F P, Jüngst T, Hennink W E, Dhert W J A, Groll J and Hutmacher D W 2013 25th anniversary article: Engineering hydrogels for biofabrication *Adv. Mater.* **25** 5011–28
- [3] Melchels F P W, Domingos M A N, Klein T J, Malda J, Bartolo P J and Hutmacher D W 2012 Additive manufacturing of tissues and organs *Prog. Polym. Sci.* **37** 1079–104
- [4] Ingber D E 2002 Mechanical signaling and the cellular response to extracellular matrix in angiogenesis and cardiovascular physiology *Circ. Res.* **91** 877–87
- [5] Bancroft G N, Sikavitsas V I, van den Dolder J, Sheffield T L, Ambrose C G, Jansen J A and Mikos A G 2002 Fluid flow increases mineralized matrix deposition in 3D perfusion culture of marrow stromal osteoblasts in a dose-dependent manner. *Proc. Natl. Acad. Sci. U. S. A.* **99** 12600–5
- [6] Markstedt K, Mantas A, Tournier I, Martínez Ávila H, Hägg D and Gatenholm P 2015 3D bioprinting human chondrocytes with nanocellulose-alginate bioink for cartilage tissue engineering applications *Biomacromolecules* **16** 1489–96
- [7] Murphy S V. and Atala A 2014 3D bioprinting of tissues and organs *Nat. Biotechnol.* **32** 773–85
- [8] Van Der Have T . and Jong G De 1996 Adult Size in Ectotherms: Temperature Effects on Growth and Differentiation *J. theor. Biol* **183** 329–40
- [9] Wang Z, Boddeda A, Parker B, Samanipour R, Ghosh S, Menard F and Kim K 2017 A high-resolution mini-microscope system for wireless real-time monitoring *IEEE Trans. Biomed. Eng.* 1–1
- [10] Kim S B, Koo K, Bae H, Dokmeci M R, Hamilton G A, Bahinski A, Kim S M, Ingber D E and Khademhosseini A 2012 A mini-microscope for in situ monitoring of cells *Lab Chip* **12** 3976

- [11] Hild W A, Breunig M and Goepferich A 2008 Quantum dots Nano-sized probes for the exploration of cellular and intracellular targeting *Eur. J. Pharm. Biopharm.* **68** 153–68
- [12] Correa D, Somoza R A and Caplan A I 2017 Non-destructive/non-invasive imaging evaluation of cellular differentiation progression during in vitro MSC-derived chondrogenesis. *Tissue Eng. Part A* ten.TEA.2017.0125
- [13] Lamping S R, Zhang H, Allen B and Ayazi Shamlou P 2003 Design of a prototype miniature bioreactor for high throughput automated bioprocessing *Chem. Eng. Sci.* **58** 747–58
- [14] Yardley J E, Kell D B, Barrett J and Davey C L 2000 On-line, real-time measurements of cellular biomass using dielectric spectroscopy. *Biotechnol. Genet. Eng. Rev.* **17** 3–35
- [15] Ansorge S, Esteban G and Schmid G 2007 On-line monitoring of infected Sf-9 insect cell cultures by scanning permittivity measurements and comparison with off-line biovolume measurements *Cytotechnology* **55** 115–24
- [16] Maskow T, Röllich A, Fetzer I, Yao J and Harms H 2008 Observation of non-linear biomass-capacitance correlations: Reasons and implications for bioprocess control *Biosens. Bioelectron.* **24** 123–8
- [17] Maskow T, Röllich A, Fetzer I, Ackermann J U and Harms H 2008 On-line monitoring of lipid storage in yeasts using impedance spectroscopy *J. Biotechnol.* **135** 64–70
- [18] McRae D a and Esrick M a 1996 Deconvolved electrical impedance spectra track distinct cell morphology changes. *IEEE Trans. Biomed. Eng.* **43** 607–18
- [19] Laufer S, Ivorra A, Reuter V E, Rubinsky B and Solomon S B 2010 Electrical impedance characterization of normal and cancerous human hepatic tissue *Physiol. Meas.* **31** 995–1009
- [20] Patel P and Markx G H 2008 Dielectric measurement of cell death *Enzyme Microb. Technol.* **43** 463–70
- [21] Angersbach A, Heinz V and Knorr D 1999 Electrophysiological model of intact and processed plant tissues: Cell disintegration criteria *Biotechnol. Prog.* **15** 753–62
- [22] Wyllie A H 1997 Apoptosis: an overview **53** 451–65
- [23] Carvell J P and Dowd J E 2006 On-line Measurements and Control of Viable Cell Density in Cell Culture Manufacturing Processes using Radio-frequency Impedance Cytotechnology **50** 35–48
- [24] Ducommun P, Kadouri A, Von Stockar U and Marison I W 2001 On-line determination of animal cell concentration in two industrial high-density culture processes by dielectric spectroscopy *Biotechnol. Bioeng.* 77 316–23
- [25] Cannizzaro C, Gügerli R, Marison I and Von Stockar U 2003 On-Line Biomass Monitoring of CHO Perfusion Culture With Scanning Dielectric Spectroscopy *Biotechnol. Bioeng.* **84** 597–610
- [26] Heileman K, Daoud J and Tabrizian M 2013 Dielectric spectroscopy as a viable biosensing tool for cell and tissue characterization and analysis *Biosens. Bioelectron.* **49** 348–59
- [27] Davey C L, Davey H M, Kell D B and Todd R W 1993 Introduction to the dielectric

- estimation of cellular biomass in real time, with special emphasis on measurements at high volume fractions *Anal. Chim. Acta* **279** 155–61
- [28] Zhang M I N, Repo T, Willison J H M and Sutinen S 1995 Electrical impedance analysis in plant tissues: on the biological meaning of Cole-Cole alpha in Scots pine needles Eur. Biophys. J. 24 99–106
- [29] Siano S A 1997 Biomass measurement by inductive permittivity *Biotechnol. Bioeng.* **55** 289–304
- [30] Ansorge S, Esteban G and Schmid G 2010 Multifrequency permittivity measurements enable on-line monitoring of changes in intracellular conductivity due to nutrient limitations during batch cultivations of CHO cells *Biotechnol. Prog.* **26** 272–83
- [31] Khamzin A A, Nigmatullin R R and Popov□ I I 2012 Microscopic Model of a Non-Debye Dielectric Relaxation: the Cole Cole Law and Its Generalization *Theor. Math. Phys.* **173** 1604–19
- [32] Narayanan L K, Huebner P, Fisher M B, Spang J T, Starly B and Shirwaiker R A 2016 3D-Bioprinting of Polylactic Acid (PLA) Nanofiber–Alginate Hydrogel Bioink Containing Human Adipose-Derived Stem Cells ACS Biomater. Sci. Eng. 2 1732–42
- [33] Doube M, Kłosowski M M, Arganda-Carreras I, Cordelières F P, Dougherty R P, Jackson J S, Schmid B, Hutchinson J R and Shefelbine S J 2010 BoneJ: Free and extensible bone image analysis in ImageJ *Bone* **47** 1076–9
- [34] Henry O, Ansorge S, Aucoin M, Voyer R and Kamen A 2007 On-Line Monitoring Of Cell Size Distribution In Mammalian Cell Culture Processes *IFAC Proc. Vol.* **40** 277–82
- [35] Nair K, Gandhi M, Khalil S, Yan K C, Marcolongo M, Barbee K and Sun W 2009 Characterization of cell viability during bioprinting processes *Biotechnol. J.* **4** 1168–77
- [36] Chang R, Nam J and Sun W 2008 Effects of Dispensing Pressure and Nozzle Diameter on Cell Survival from Solid Freeform Fabrication–Based Direct Cell Writing *Tissue Eng.* Part A 14 41–8
- [37] Asami K 2002 Characterization of heterogeneous systems by dielectric spectroscopy *Prog. Polym. Sci.* **27** 1617–59
- [38] Daoud J, Asami K, Rosenberg L and Tabrizian M 2012 Dielectric spectroscopy for non-invasive monitoring of epithelial cell differentiation within three-dimensional scaffolds Phys. Med. Biol. 57 5097–112
- [39] Buyukhatipoglu K, Jo W, Sun W and Clyne A M 2009 The role of printing parameters and scaffold biopolymer properties in the efficacy of a new hybrid nano-bioprinting system *Biofabrication* **1** 35003
- [40] Lin Y, Huang G, Huang Y, Jeremy Tzeng T and Chrisey D 2010 Effect of laser fluence in laser-assisted direct writing of human colon cancer cell ed D Bourell *Rapid Prototyp. J.* **16** 202–8
- [41] Ali M, Pages E, Ducom A, Fontaine A and Guillemot F 2014 Controlling laser-induced jet formation for bioprinting mesenchymal stem cells with high viability and high resolution *Biofabrication* **6** 45001
- [42] Kattamis N T, Purnick P E, Weiss R and Arnold C B 2007 Thick film laser induced

- forward transfer for deposition of thermally and mechanically sensitive materials *Appl. Phys. Lett.* **91** 171120
- [43] Ozbolat I T and Yin Yu 2013 Bioprinting Toward Organ Fabrication: Challenges and Future Trends *IEEE Trans. Biomed. Eng.* **60** 691–9
- [44] Narayanan L K, Huebner P, Fisher M B, Spang J T, Starly B and Shirwaiker R A 2016 3D-Bioprinting of Polylactic Acid (PLA) Nanofiber–Alginate Hydrogel Bioink Containing Human Adipose-Derived Stem Cells *ACS Biomater. Sci. Eng.* **2** 1732–42
- [45] Duan B, Hockaday L A, Kang K H and Butcher J T 2013 3D Bioprinting of heterogeneous aortic valve conduits with alginate/gelatin hydrogels *J. Biomed. Mater. Res. Part A* **101A** 1255–64
- [46] Canali C, Heiskanen A, Muhammad H B, Høyum P, Pettersen F-J, Hemmingsen M, Wolff A, Dufva M, Martinsen Ø G and Emnéus J 2015 Bioimpedance monitoring of 3D cell culturing—Complementary electrode configurations for enhanced spatial sensitivity *Biosens. Bioelectron.* **63** 72–9
- [47] Lee S-M, Han N, Lee R, Choi I-H, Park Y-B, Shin J-S and Yoo K-H 2016 Real-time monitoring of 3D cell culture using a 3D capacitance biosensor *Biosens. Bioelectron.* **77** 56–61
- [48] Faulkner-Jones A, Fyfe C, Cornelissen D-J, Gardner J, King J, Courtney A and Shu W 2015 Bioprinting of human pluripotent stem cells and their directed differentiation into hepatocyte-like cells for the generation of mini-livers in 3D *Biofabrication* **7** 44102
- [49] Gao G, Schilling A F, Hubbell K, Yonezawa T, Truong D, Hong Y, Dai G and Cui X 2015 Improved properties of bone and cartilage tissue from 3D inkjet-bioprinted human mesenchymal stem cells by simultaneous deposition and photocrosslinking in PEG-GelMA *Biotechnol. Lett.* **37** 2349–55
- [50] Bagnaninchi P O and Drummond N 2011 Real-time label-free monitoring of adiposederived stem cell differentiation with electric cell-substrate impedance sensing. *Proc. Natl. Acad. Sci. U. S. A.* **108** 6462–7
- [51] Nordberg R C, Zhang J, Griffith E H, Frank M W, Starly B and Loboa E G 2016 Electrical Cell-Substrate Impedance Spectroscopy Can Monitor Age-Grouped Human Adipose Stem Cell Variability During Osteogenic Differentiation. *Stem Cells Transl. Med.* sctm.2015-0404
- [52] Zeiser A, Bedard C, Voyer R, Jardin B, Tom R and Kamen A A 1999 On-line monitoring of the progress of infection in Sf-9 insect cell cultures using relative permittivity measurements *Biotechnol. Bioeng.* **63** 122–6
- [53] Wang Z, Abdulla R, Parker B, Samanipour R, Ghosh S and Kim K 2015 A simple and high-resolution stereolithography-based 3D bioprinting system using visible light crosslinkable bioinks *Biofabrication* **7** 45009
- [54] Ma X, Qu X, Zhu W, Li Y-S, Yuan S, Zhang H, Liu J, Wang P, Lai C S E, Zanella F, Feng G-S, Sheikh F, Chien S and Chen S 2016 Deterministically patterned biomimetic human iPSC-derived hepatic model via rapid 3D bioprinting. *Proc. Natl. Acad. Sci. U. S. A.* **113** 2206–11
- [55] de Gans B-J, Duineveld P C and Schubert U S 2004 Inkjet Printing of Polymers: State of the Art and Future Developments *Adv. Mater.* **16** 203–13